Journal of Materials Chemistry

Cite this: J. Mater. Chem., 2011, 21, 18738

www.rsc.org/materials

PAPER

Electrochromism of rutile nanowires, vertically aligned along the [001] direction, due to alkali metal ion intercalation†

Min-Han Yang,[a] Ting-Ting Chen,[a] Yu-Shiuan Wang,[a] Hsin-Tien Chiu[c] and Chi-Young Lee*[ab]

Received 4th July 2011, Accepted 14th September 2011
DOI: 10.1039/c1jm13084f

Rutile nanowires were grown along the [001] direction and perpendicular to the fluorine doped tin oxide coated glass substrate ($R_\perp$) by a solvothermal process using titanium isopropoxide as the precursor in acidic solution. The edge length of the nanowires obtained in isopropyl alcohol is ten times less than that of the nanowires obtained in water. Due to the high ionic diffusion rate along the rutile [001] direction and good optical transmittance, $R_\perp$ was used as an electrochromism electrode. When −2 V was applied, the color of the electrode became blue with a 60% change in the transmittance for 30 s due to the cathodic polarization potential in $LiClO_4$/PC electrolyte (where PC is propylene carbonate). The lithium ion intercalated/extracted densities of $R_\perp$, P25-coated and rutile nanowires-coated electrodes are 138.6/129.1 mC cm^{-2}, 93.6/83.2 mC cm^{-2} and 31.7/15.9 mC cm^{-2} respectively. After 50 cycles, the $R_\perp$ electrode still performs very well. Furthermore, a large amount of sodium cation intercalation into TiO_2 was observed for the first time at −1.0 V. According to these results, the $R_\perp$ electrode is a promising candidate to be a multi-function device.

Introduction

Recently, titanium dioxide has received more attention due to its peculiar properties such as chemical stability, being environmentally friendly and being low cost. It has a variety of applications in photocatalysis,[1–3] dye sensitized solar cells,[4–6] lithium ion storage[7–10] and electrochromic devices.[11–13]

Electrochromic devices such as smart window, e-paper displays, and so on,[14–17] can be associated with cathodic[18–20] and anodic[21] coloration. TiO_2 exhibits cathodic coloration due to cation intercalation into TiO_2 lattices under cathodic polarization potential. The cathodic polarization potential reduces Ti^{4+} to Ti^{3+},[22] resulting in a decrease of the band gap, which leads to the coloration of TiO_2.[23] When an opposite voltage is applied, the cations are extracted out of the TiO_2 lattices which leads to the color fading away. Therefore, the coloration can be switched by reversing the voltage. Moreover, there is close relation between electrochromism and lithium ion energy storage for TiO_2, as both are concerned with cation intercalation/extraction. For electrochromism and lithium ion energy storage, the performances are related to the quantity of cation intercalation, which is strongly affected by the diffusion velocity of cations in TiO_2. It was reported that the theoretical diffusion coefficients for Li^+ along the [001] direction of rutile is 10^{-6} cm^2 s^{-1} and the [110] direction of rutile is 10^{-15} cm^2 s^{-1}.[24,25] For anatase phase TiO_2, the diffusion coefficient along the [101] direction is about 10^{-13} cm^2 s^{-1}.[26]

According to literature,[13,27,28] TiO_2 nanoparticles and nanoporous structures provided high surface areas on conductive substrates, which are usually used to make electrochromic devices. Recently, an electrochromic device made using anodic TiO_2 nanotubes on Ti foil was studied by P. Schmuki *et al.*[29,30] Owing to the large surface area and good contact between TiO_2 and substrate, the TiO_2 nanotubes electrode shows good electrochromic optical performance. However, the method discussed above must use a high temperature annealing process to remove binders and improve the crystallinity of TiO_2.

In this research work, we attempt to form an electrode with vertically aligned rutile nanowires along the [001] direction (with the advantageous rutile [001] one-dimensional structure) perpendicular to fluorine doped tin oxide coated glass (FTO) by a simple one step solvothermal process. The electrochromism and alkali metal ion intercalation properties are studied in detail.

Experimental section

Vertically aligned rutile nanowires grown on FTO

15 ml of concentrated hydrochloric acid (37%, Aldrich) and 15 ml of isopropyl alcohol (IPA, J.T.baker) were mixed and 1 ml

[a]Department of Materials Science and Engineering, National Tsing Hua University, Hsinchu, Taiwan, 30013, R. O. C. E-mail: cylee@mx.nthu.edu.tw; Fax: +886 3571 3113; Tel: +886 3572 8692
[b]Center for Nanotechnology, Materials Science, and Microsystems, National Tsing Hua University, Hsinchu, Taiwan, 30013, R. O. C; Fax: +886 3571 3113; Tel: +886 3572 8692
[c]Department of Applied Chemistry, National Chiao Tung University, Hsinchu, Taiwan, 300, R. O. C. E-mail: htchiu@cc.nctu.edu.tw; Fax: +886 3571 3113; Tel: +886 3513 1514
† Electronic supplementary information (ESI) available. See DOI: 10.1039/c1jm13084f

titanium isopropoxide (TTIP, 98%, Aldrich) was added as the precursor solution. The fluorine doped tin oxide coated glass (FTO, 10 ohm per square) was cleaned by sonication for 15 min in acetone, ethanol, DI water and IPA sequentially. The FTO was placed within a Teflon reactor and the precursor solution was added, then the Teflon reactor was loaded in the autoclave and placed in an oven. The synthetic condition was controlled at 180 °C for 5 min to 4 h. After the solvothermal reaction, the sample was taken out, washed with DI water and dried in ambient air. The electrode obtained by 4 h reaction was designated as $R_{\perp}$ and used for an electrochemical test.

Coating TiO_2 film onto FTO

Powders of commercial P25 (75% anatase and 25% rutile) and rutile nanowires synthesized in our laboratory[2] were used as the reference samples. 0.25 g mL^{-1} TiO_2 and 0.25 g mL^{-1} polyethylene glycol (PEG, 35 K) were mixed completely using mixing equipment until a paste formed. These TiO_2 pastes were coated onto FTO. Then the TiO_2 film was heated in air at 450 °C for 30 min to remove organics and bind the TiO_2 film on the FTO. All the TiO_2 films were of the same thickness (*ca.* 4 μm, Fig. S1 in the Supporting Information†). The P25-coated and rutile-nanowire-powder coated electrodes are referred to as P25 and $R_{\parallel}$, respectively.

Materials characterization

The morphologies of the materials were examined by FE-SEM (JSE-6500F field emission SEM). The high resolution morphological analyses were performed by HRTEM (JEOL 2010). Phase detection analysis was studied by XRD pattern (Brucker D8-advanced with Cu-Kα radiation $\lambda = 1.5405981$ Å). A Raman spectrometer (Renishaw, using the laser with $\lambda = 632.8$ nm) was used to characterize the structure of the samples.

Electrochromic performance

The electrochromic properties of TiO_2 electrodes were examined using an electrochemical system (AUTOLAB, PGSTAT30) and an UV-visible system (Avantes UV spectrum). The electrochemical system was used with a three-electrode cell setup. To study the intercalation of cations (Li^+, Na^+), the three electrodes TiO_2–FTO, Ag/AgCl, and Pt wire as working, reference and counter electrode, respectively, were immersed in electrolytic solutions such as 1 M $LiClO_4$ (anhydrous, Alfa Aesar) and 1 M $NaClO_4$ (anhydrous, Alfa Aesar) in propylene carbonate (PC, 99%, Alfa Aesar). The chronoamperometric measurements were performed using an Autolab electrochemical system. The coloration of TiO_2 was measured using a UV-visible system.

Results and discussion

Fig. 1 represents the characterization of TiO_2 grown on FTO by reacting TTIP in IPA. Fig. 1(a)–(b) shows vertically aligned uniform TiO_2 rectangular prisms with 20 nm edge lengths and 3.8 μm height, which were obtained at 180 °C for 4 h reaction. Fig. 1(c) shows the Raman shift for samples for different reaction times. The peaks appearing at 240, 450, and 615 cm^{-1} correspond to a multi-photon process, E_g and A_{1g} vibrational modes of TiO_2

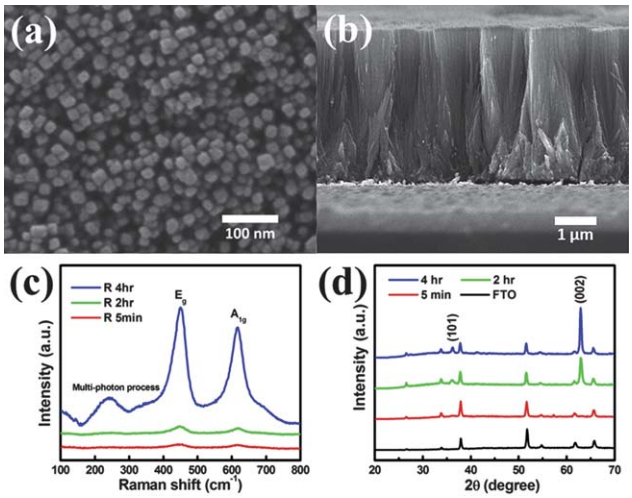

Fig. 1 Characterization of vertically aligned rutile nanowires grown on FTO: FESEM images of (a) top-view (b) cross-section; (c) Raman spectra (d) X-ray diffraction patterns for different reaction times from 5 min to 4 h.

rutile phase, respectively.[31] It can be seen that the rutile phase formed with in the first 5 min. The X-ray diffraction pattern (Fig. 1(d)) indicates that the 2θ values, 36.2°, 62.9° reflecting from the (101), (002) lattice planes of rutile TiO_2 (JCPDS 89-4920, $P4_2/mnm$, $a = b = 0.4584$ nm and $c = 0.2953$ nm), and the intensities of the peaks increase with the reaction time (5 min to 4 h). Moreover, the intensity of the peak reflecting from the (002) planes increases most noticably. It suggests that the rutile nanowires were well crystallized along the (002) axes. Rutile nanowires were grown on FTO without any seeding process, owing to the lattice match between FTO ($a = b = 0.4687$ nm) and the rutile phase TiO_2.[32,33]

Fig. 2(a)–(b) shows low-magnification transmission electron microscopic images of a bundle rutile nanowires. Fig. 2(c) shows a TEM image of an isolated rutile nanowire. Fig. 2(d) displays an HRTEM image of the region marked in red in Fig. 2(c), and the

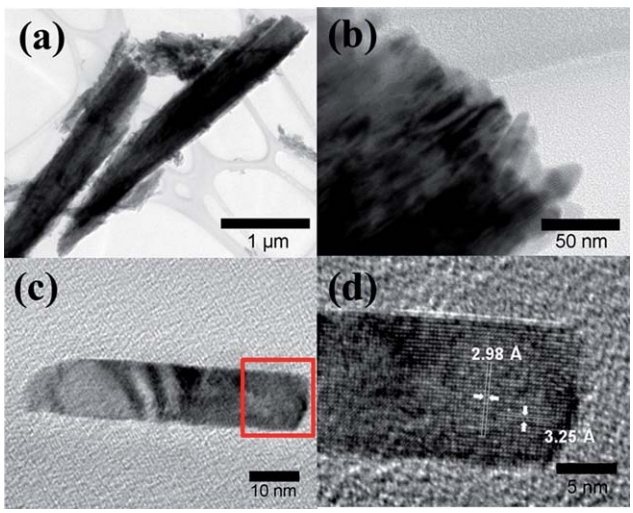

Fig. 2 TEM images of rutile nanowires: (a) and (b) are bundles, (c) is an isolated rutile nanowire, and (d) is an HRTEM image of the area marked in red in (c).

fringes from the {001} and {110} planes, revealing *d* spacings of 2.98 Å and 3.25 Å, respectively. It shows that, the growth direction of rutile nanowires proceeds along [001], and the circumambient surface is {110}. These observations were consistent with the XRD pattern, indicating that the rutile nanowires grew vertically on FTO along the [001] lattice. According to the literature,[2,34–36] Cl ions play an important role in the growth of rutile. In a rutile crystal, each TiO_6 octahedron shares two opposing edges which are adjacent to another neighbor edge in a linear chain structure. Once the {110} plane of rutile was exposed in the hydrogen chloride solution, Cl ions were adhered on the {110} surface and restricting the sideways growth. This leads to the growth rate along [110] being slower than that along the [001] direction, resulting in the anisotropic growth of rutile TiO_2 along the [001] direction.

According to the literature,[33,37–39] rutile nanowires on FTO have been synthesized by hydrothermal reaction. Fig.3(a)–(b) and 3(d)–(e) show the SEM images of rutile nanowires on FTO obtained in IPA and water. The edge length of rutile nanowires obtained in IPA is *ca.* 20 nm, and the edge length is *ca.* 200 nm when using water as the solvent. The edge length of the nanowires obtained in isopropyl alcohol is ten times less than that of those obtained in water. The TiO_2 precursor prefers to dissolve in a low polarity solvent like IPA, rather than in water, resulting in lower surface energy of the growing material, which leads to the growth of tiny rods.[40] Fig. 3(c) and (f) show the different transmittance of the samples obtained in IPA and water. According to the optical images (Fig. 3(c)), "NTHU" can be seen clearly through rutile nanowires grown in IPA (left) but not through those grow in H_2O (right). Fig. 3(f) shows the UV-visible spectra of the two samples. The transmittance of wavelengths below 380 nm is zero owing to the band gap (~3.0 eV) of TiO_2. The transmittance of rutile nanowires that were grown in IPA increases gradually with increasing wavelength. At $\lambda = 750$ nm, the transmittances of rutile nanowires grown in IPA and H_2O are 48% and 7%, respectively.

The rutile electrode grown in IPA ($R_\perp$) was colored by supplying a voltage in 1 M $LiClO_4$/PC solution.[41] The electrochromism and ionic intercalation behavior of $R_\perp$ was studied in detail, and compared with the electrodes made by conventional methods, such as P25 and rutile nanowire powder ($R_\parallel$).

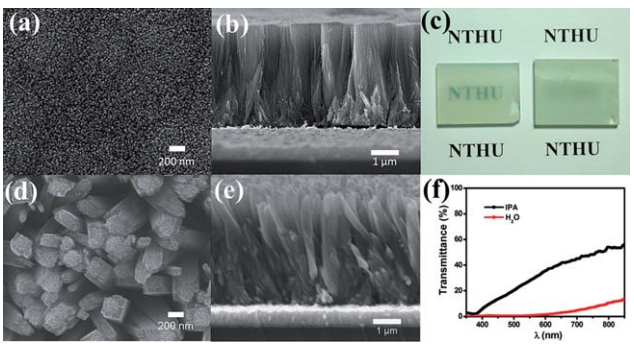

Fig. 3 FESEM images of rutile nanowires grown on FTO from different solvents; IPA and H_2O. (a) and (b) show the top-view and cross-section of rutile nanowires in IPA, respectively. (c) shows a photographic image of the rutile electrode in IPA (left) and in H_2O (right). (d) and (e) show the top-view and cross-section, respectively, of rutile nanowires in H_2O. (f) UV-visible spectrum of the rutile electrodes.

There is no obvious reduction and oxidation peak in the cyclic voltammogram, the cyclic voltammograms for different scan rates strongly imply that this is a diffusion controlled reaction,[42] as shown in Fig. S2 in the Supporting Information.† Fig. 4 presents the electrochromic behaviors of the $R_\perp$ electrode in 1 M $LiClO_4$/PC electrolyte. Fig. 4(a) indicates the coloration of $R_\perp$ with different cathodic polarization potentials which are 0 V, −1 V, −1.5 V and −2 V relative to Ag/AgCl. Compared with the semi-transparency of $R_\perp$, the color of the electrode becomes deep blue as the cathodic polarization potentials are increased. Fig. 4(b) shows the transmittance spectra of $R_\perp$ with and without applying −1.5 V voltage. When −1.5 V voltage was applied, $R_\perp$ showed a maximum peak of transmittance at $\lambda = 500$ nm and the transmittance gradually decreased from the visible region to the near infrared. According to the literature,[23,43] additional electronic states about 0.75 and 1.18 eV below the conduction band of TiO_2 are produced due to the reduction of TiO_2. Therefore, the coloration of the TiO_2 electrode is partly due to the visible region tail of the infrared adsorption peak of reduced TiO_2. Fig. 4(c) shows the cycling stability of $R_\perp$ by showing the transmittance at $\lambda = 750$ nm over 50 cycles (0 to −1.5 V for 30 s). Over the whole experiment period, the uncolored transmittance is 62%, which becomes 12% after coloration. Throughout the experiment, the electrode maintains good electrochromic performance. Fig. 4(d) shows the charging and discharging plots over 50 cycles. At the first cycle, the estimated charge and discharge densities (Q_c and Q_d) are 71.03 mC cm^{-2} and 55.44 mC cm^{-2}, respectively; and the reversibility ratio (Q_c/Q_d) is 78%. The reversibility of the second cycle increased to 87%. This may be due to a reaction at the surface of the rutile nanowires. We will be addressing these aspects in our future work.

The coloration and lithium ion intercalation/extraction of various TiO_2 electrodes were further investigated by applying different cathodic polarization potentials, as shown in Fig. 5. Fig. 5(a) shows the transmittance of TiO_2 electrodes for cathodic polarization potentials from 0.75 to 2.00 V. The uncolored

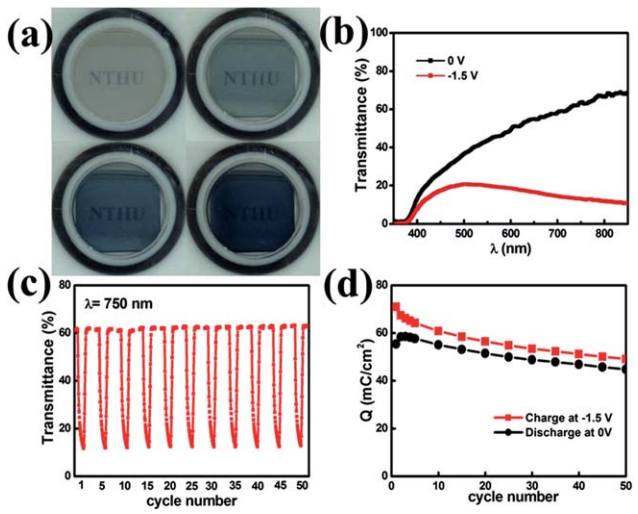

Fig. 4 (a) Photographic image of the coloration of $R_\perp$ electrode with different cathodic polarization potentials (0 V, −1 V, −1.5 V and −2 V) for 30 s in 1 M $LiClO_4$/PC. (b) Transmittance spectrum of $R_\perp$ electrode (0/−1.5 V for 30 s). (c) Multiple cycle behavior of $R_\perp$ electrode transmittance. (d) Charging/discharging at 750 nm for 50 cycles.

transmittance at $\lambda = 750$ nm is 62%, 32% and 12% for $R_\perp$, P25 and $R_\parallel$, respectively. The transmittance of $R_\perp$ is much higher than that of P25 and $R_\parallel$. Random arrangement of powdered P25 and rutile nanowires powder resulted in higher scattering of light, which leads to lower transmittance of the electrodes. The threshold polarization is above −1.25 V for P25 and $R_\parallel$, whereas it is −1.00 V for $R_\perp$. The coloration performance of all TiO_2 electrodes are shown in the supporting information, as shown in Fig. S3.† The coloration ability of these electrodes can be estimated using the equation[44]

$$\Delta OD = \log (T_{\text{bleaching}}/T_{\text{coloring}}) \quad (1)$$

Where ΔOD is optical density change, $T_{\text{bleaching}}$ is uncolored transmittance, and T_{coloring} is transmittance with coloration at $\lambda = 750$ nm). From Fig. 5(b), the ΔOD values at −2 V are 1.45, 1.32 and 0.29 for $R_\perp$, P25 and $R_\parallel$, respectively. Moreover, $R_\perp$ has the largest values of ΔOD among the TiO_2 materials at different cathodic polarization potentials. The color switching responses of the films were estimated by calculating the differential of the transmittance *versus* time, as shown in Fig. S4.† $R_\perp$ again has the largest peak height and the narrowest peak width among the TiO_2 materials at different cathodic polarization potentials. Fig. 5(c) shows current response for a series of different cathodic polarization potentials. The values (Fig. 5(d)) of charge/discharge are 138.6/129.1 mC cm^{-2} for $R_\perp$, 93.6/83.2 mC cm^{-2} for P25, and 31.7/15.9 mC cm^{-2} for $R_\parallel$ at −2 V charging for 30 s. This suggests that the electrode made by $R_\perp$ shows the highest electric charge and discharge density among these three titanium dioxides. This property is most important for high rate energy storage materials.[45] Furthermore, the electrochromic efficiency (η) has been estimated using the equation

$$\eta = \Delta T/Q_c \ (\text{cm}^2\ \text{C}^{-1}) \quad (2)$$

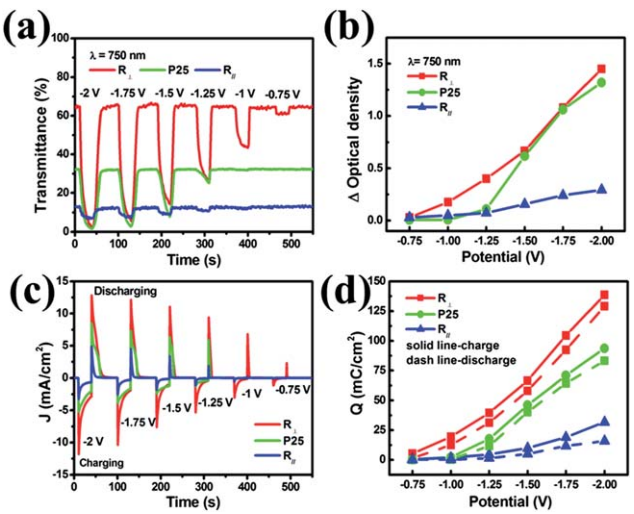

Fig. 5 The electrochromic measurements of TiO_2 electrodes ($R_\perp$, P25, $R_\parallel$) at a series of cathodic polarization potentials (from 0 V to −2 V) in 1 M $LiClO_4$/PC. The optical characteristics (a) transmittance change and (b) the optical density change. The electric characteristics are (c) chronoamperometry and (d) electric charge density (solid line = charge, dashed line = discharge).

Where $\Delta T = T_{\text{bleaching}} - T_{\text{coloring}}$ at 750 nm, Q_c is the charge density at −2 V charging for 30 s. The electrochromic efficiencies are 452.3 $cm^2\ C^{-1}$ for $R_\perp$, 329.7 $cm^2\ C^{-1}$ for P25, and 203.0 $cm^2\ C^{-1}$ for $R_\parallel$ at −2 V charging for 30 s.

The lithium ion intercalation performance of $R_\perp$ is better than that of other materials, which can be attributed to the different ion diffusion coefficients of TiO_2. It was reported that the theoretical diffusion coefficients for Li^+ of rutile along the [001] and [110] direction are 10^{-6} and 10^{-15} $cm^2\ s^{-1}$, respectively.[24,25] According to

$$x \approx \sqrt{Dt} \quad (3)$$

Where x is the mean square displacement, D is the diffusion coefficient, and t is the diffusion time. The mean square displacement per second is 10 μm for $rutile_{[001]}$, 3.2 Å for $rutile_{[110]}$.[7] Scheme 1 shows that the rutile grown vertically along [001] on FTO substrate results in the parallel of its [001] direction and the direction of electric potential gradient, which leads to rapid diffusion of lithium ions through the [001] channel. In addition, the characteristics of one-dimensional structure and good connection between rutile nanowires and FTO substrate markedly enhance the electron transport.[20,46–48] However, for $R_\parallel$, the rutile nanowires powder is coated on FTO substrate in which most of the nanowires tends to lie on the substrate due to the wire morphology, resulting in the [110] direction of rutile nanowires being parallel to the direction of the electric potential gradient. See Scheme 1. The small diffusion coefficient along the rutile [110] direction reduces the lithium ion diffusion through the [110] direction, leading to less charge intercalation and extraction for $R_\parallel$. From Fig. 5(c), the $R_\perp$ electrode showes a much higher current density (−11.8 mA cm^{-2}) than that of the $R_\parallel$ (−3.3 mA cm^{-2}) when −2.00 V is supplied. Moreover, the low diffusion along the rutile [110] direction also causes trapping of electrons, which leads to low reversibility (50%) of $R_\parallel$. P25, the anatase phase dominated material with a 10^{-13} $cm^2\ s^{-1}$ diffusion coefficient,[26] shows a reasonable charge intercalation/extraction behavior. In addition, the reported energy barriers of Li^+

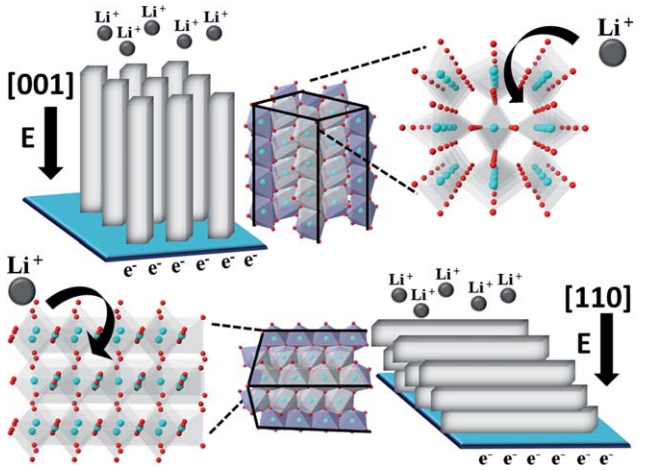

Scheme 1 The delineation of Li^+ intercalation through [001] and [110] direction corresponds to $R_\perp$ and $R_\parallel$, respectively. (O atoms are shown as red spheres, Ti atoms are shown as blue spheres, and Li^+ are shown as grey spheres).

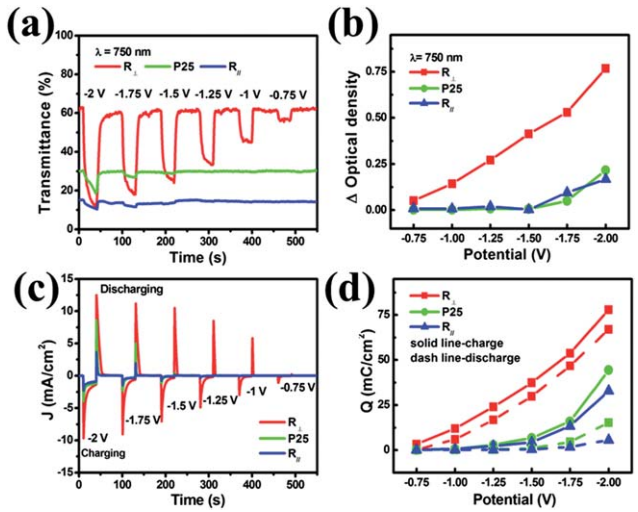

Fig. 6 The chronoamperometric measurements for TiO_2 electrodes ($R_\perp$, P25, $R_\parallel$) at a series of cathodic polarization potentials (from 0 V to −2 V) in 1 M $NaClO_4$/PC. The optical characteristics (a) transmittance change and (b) the optical density change. The electric characteristics (c) chronoamperometry and (d) electric charge density (solid line = charge, dash line = discharge).

transport are 0.39 to 0.65 eV for anatase and 0.04 to 0.22 eV for the rutile [001] direction,[49,50] which are also consist with our observations.

Owing to the existing large diffusion channel perpendicular to FTO, sodium ion intercalation through $R_\perp$ was also investigated (Fig. 6). According to the literature,[51,52] commercial P25 and anatase phase TiO_2 nanotubes cannot be colored in $NaClO_4$/PC at −1.5 V, on account of the size of the sodium ions. On the other hand, niobium doped anatase TiO_2 with widened lattice made sodium ion intercalation possible.[51] Unexpectedly, $R_\perp$ shows an obvious coloration and cation intercalation at −1.00 V. In addition, when cathodic polarization potential is applied up to −1.75 V, P25 and $R_\parallel$ had an observable coloration and cation intercalation as shown in Fig. 6. This implies that the energy barrier for sodium ions to intercalate into $R_\perp$ is much less than that for other electrodes. From Fig. 6(b) and 6(d), the ΔOD values and charge intercalations of $R_\perp$ are much larger than those of P25 and $R_\parallel$ at a series of different cathodic polarization potentials. At −2 V, the charge/discharge densities are 77.9/67.0 mC cm^{-2} for $R_\perp$, 44.4/15.2 mC cm^{-2} for P25, and 32.8/5.6 mC cm^{-2} for $R_\parallel$. Moreover, the reversibility ratios are 86%, 34% and 17% for $R_\perp$, P25 and $R_\parallel$, respectively.

Conclusions

In summary, rutile nanowires along [001] direction vertically aligned on FTO ($R_\perp$) was synthesized by using IPA as solvent under solvothermal conditions. At λ = 750 nm, the transmittances of rutile nanowires grown in IPA and in H_2O are 48% and 7%, respectively. Due to the ultrahigh ionic diffusion coefficient of rutile along the [001] direction, lithium ions can rapidly diffuse through the [001] direction, which is parallel to the electric potential gradient. The change in optical density at −2 V for 30 s is 1.45, 1.32 and 0.29 for $R_\perp$, P25 and $R_\parallel$, respectively. In addition, the lithium ion intercalated/extracted densities of $R_\perp$, P25-coated and rutile nanowires-coated electrodes are 138.6/129.1 mC cm^{-2}, 93.6/83.2 mC cm^{-2} and 31.7/15.9 mC cm^{-2} respectively. Moreover, the $R_\perp$ electrode also shows good stability over multiple cycles. Furthermore, $R_\perp$ demonstrates an obvious coloration and sodium ion intercalation at −1.0 V, whereas P25 and $R_\parallel$ show coloration at −1.75 V. In addition to good performance in coloration and cation intercalation, $R_\perp$ also shows good electric reversibility. The electric reversibility ratios are 86%, 34% and 17% for $R_\perp$, P25 and $R_\parallel$, respectively. $R_\perp$ electrode with significant performance in electrochromism and alkali metal ion intercalation/extraction is a promising candidate for being a multifunction device. This result implies that the high speed diffusion channel of a crystal coordinates with the direction of the electric potential gradient resulting in the splendid performance of ion intercalation/extraction, which may be widely used in the synthesis of different devices.

References

1 R. Asahi, T. Morikawa, T. Ohwaki, K. Aoki and Y. Taga, *Science*, 2001, **293**, 269–271.
2 T. Y. Ke, C. W. Peng, C. Y. Lee, H. T. Chiu and H. S. Sheu, *CrystEngComm*, 2009, **11**, 1691–1695.
3 X. Feng, J. D. Sloppy, T. J. LaTempa, M. Paulose, S. Komarneni, N. Bao and C. A. Grimes, *J. Mater. Chem.*, 2011, **21**, 13429–13433.
4 B. Oregan and M. Gratzel, *Nature*, 1991, **353**, 737–740.
5 U. Bach, D. Lupo, P. Comte, J. E. Moser, F. Weissortel, J. Salbeck, H. Spreitzer and M. Gratzel, *Nature*, 1998, **395**, 583–585.
6 L. De Marco, M. Manca, R. Buonsanti, R. Giannuzzi, F. Malara, P. Pareo, L. Martiradonna, N. M. Giancaspro, P. D. Cozzoli and G. Gigli, *J. Mater. Chem.*, 2011, **21**, 13371–13379.
7 Y. S. Hu, L. Kienle, Y. G. Guo and J. Maier, *Adv. Mater.*, 2006, **18**, 1421.
8 M. C. Tsai, J. C. Chang, H. S. Sheu, H. T. Chiu and C. Y. Lee, *Chem. Mater.*, 2009, **21**, 499–505.
9 P. Kubiak, M. Pfanzelt, J. Geserick, U. Hormann, N. Husing, U. Kaiser and M. Wohlfahrt-Mehrens, *J. Power Sources*, 2009, **194**, 1099–1104.
10 T. Djenizian, I. Hanzu and P. Knauth, *J. Mater. Chem.*, 2011, **21**, 9925–9937.
11 T. Seike and J. Nagai, *Sol. Energy Mater.*, 1991, **22**, 107–117.
12 N. Ozer, *Thin Solid Films*, 1992, **214**, 17–24.
13 N. N. Dinh, N. T. T. Oanh, P. D. Long, M. C. Bernard and A. Hugot-Le Goff, *Thin Solid Films*, 2003, **423**, 70–76.
14 C. Bechinger, S. Ferrer, A. Zaban, J. Sprague and B. A. Gregg, *Nature*, 1996, **383**, 608–610.
15 U. Bach, D. Corr, D. Lupo, F. Pichot and M. Ryan, *Adv. Mater.*, 2002, **14**, 845–848.
16 W. Weng, T. Higuchi, M. Suzuki, T. Fukuoka, T. Shimomura, M. Ono, L. Radhakrishnan, H. J. Wang, N. Suzuki, H. Oveisi and Y. Yamauchi, *Angew. Chem., Int. Ed.*, 2010, **49**, 3956–3959.
17 D. T. Gillaspie, R. C. Tenent and A. C. Dillon, *J. Mater. Chem.*, 2010, **20**, 9585–9592.
18 S. H. Lee, H. M. Cheong, C. E. Tracy, A. Mascarenhas, A. W. Czanderna and S. K. Deb, *Appl. Phys. Lett.*, 1999, **75**, 1541–1543.
19 S. Balaji, Y. Djaoued, A.-S. Albert, R. Bruning, N. Beaudoin and J. Robichaud, *J. Mater. Chem.*, 2011, **21**, 3940–3948.
20 J. Zhang, J.-p. Tu, X.-h. Xia, X.-l. Wang and C.-d. Gu, *J. Mater. Chem.*, 2011, **21**, 5492–5498.
21 R. C. Tenent, D. T. Gillaspie, A. Miedaner, P. A. Parilla, C. J. Curtis and A. C. Dillon, *J. Electrochem. Soc.*, 2010, **157**, H318–H322.
22 M. P. Cantao, J. I. Cisneros and R. M. Torresi, *Thin Solid Films*, 1995, **259**, 70–74.
23 D. C. Cronemeyer and M. A. Gilleo, *Phys. Rev.*, 1951, **82**, 975–976.
24 M. V. Koudriachova, N. M. Harrison and S. W. de Leeuw, *Phys. Rev. Lett.*, 2001, **86**, 1275–1278.
25 O. W. Johnson, *Phys. Rev.*, 1964, **136**, A284.

26 M. Wagemaker, R. van de Krol, A. P. M. Kentgens, A. A. van Well and F. M. Mulder, *J. Am. Chem. Soc.*, 2001, **123**, 11454–11461.
27 S. Y. Choi, M. Mamak, N. Coombs, N. Chopra and G. A. Ozin, *Nano Lett.*, 2004, **4**, 1231–1235.
28 C. M. Wang and S. Y. Lin, *J. Solid State Electrochem.*, 2006, **10**, 255–259.
29 A. Ghicov, H. Tsuchiya, R. Hahn, J. M. Macak, A. G. Munoz and P. Schmuki, *Electrochem. Commun.*, 2006, **8**, 528–532.
30 R. Hahn, A. Ghicov, H. Tsuchiya, J. M. Macak, A. G. Munoz and P. Schmuki, *Phys. Status Solidi A*, 2007, **204**, 1281–1285.
31 S. P. S. Porto, P. A. Fleury and T. C. Damen, *Phys. Rev.*, 1967, **154**, 522.
32 M. Abd-Lefdil, R. Diaz, H. Bihri, M. A. Aouaj and F. Rueda, *Eur. Phys. J.: Appl. Phys.*, 2007, **38**, 217–219.
33 B. Liu and E. S. Aydil, *J. Am. Chem. Soc.*, 2009, **131**, 3985–3990.
34 E. Hosono, S. Fujihara, K. Kakiuchi and H. Imai, *J. Am. Chem. Soc.*, 2004, **126**, 7790–7791.
35 P. M. Oliver, G. W. Watson, E. T. Kelsey and S. C. Parker, *J. Mater. Chem.*, 1997, **7**, 563–568.
36 X. J. Feng, J. Zhai and L. Jiang, *Angew. Chem., Int. Ed.*, 2005, **44**, 5115–5118.
37 A. Kumar, A. R. Madaria and C. W. Zhou, *J. Phys. Chem. C*, 2010, **114**, 7787–7792.
38 H. Wang, Y. Bai, Q. Wu, W. Zhou, H. Zhang, J. Li and L. Guo, *Physical Chemistry Chemical Physics*, 2011, **13**, 7008–7013.
39 H. Wang, Y. S. Bai, H. Zhang, Z. H. Zhang, J. H. Li and L. Guo, *J. Phys. Chem. C*, 2010, **114**, 16451–16455.
40 H. G. Yang, G. Liu, S. Z. Qiao, C. H. Sun, Y. G. Jin, S. C. Smith, J. Zou, H. M. Cheng and G. Q. Lu, *J. Am. Chem. Soc.*, 2009, **131**, 4078–4083.
41 T. Berger, T. Lana-Villarreal, D. Monllor-Satoca and R. Gomez, *Chem. Phys. Lett.*, 2007, **447**, 91–95.
42 A. Ghicov, S. P. Alba, J. M. Macak and P. Schmuki, *Small*, 2008, **4**, 1063–1066.
43 D. C. Cronemeyer, *Phys. Rev.*, 1959, **113**, 1222.
44 K. Bange and T. Gambke, *Adv. Mater.*, 1990, **2**, 10–16.
45 J. S. Chen and X. W. Lou, *J. Power Sources*, 2010, **195**, 2905–2908.
46 C. K. Chan, X. F. Zhang and Y. Cui, *Nano Lett.*, 2008, **8**, 307–309.
47 J. H. Bang and P. V. Kamat, *Adv. Funct. Mater.*, 2010, **20**, 1970–1976.
48 J. Ng, J. H. Pan and D. D. Sun, *J. Mater. Chem.*, 2011, **21**, 11844–11853.
49 S. Kerisit, K. M. Rosso, Z. G. Yang and J. Liu, *J. Phys. Chem. C*, 2009, **113**, 20998–21007.
50 M. L. Sushko, K. M. Rosso and J. Liu, *J. Phys. Chem. C*, 2010, **114**, 20277–20283.
51 A. Ghicov, M. Yamamoto and P. Schmuki, *Angew. Chem., Int. Ed.*, 2008, **47**, 7934–7937.
52 S. Berger, A. Ghicov, Y. C. Nah and P. Schmuki, *Langmuir*, 2009, **25**, 4841–4844.